

DEEP RADIOMIC SIGNATURE WITH IMMUNE CELL MARKERS PREDICTS THE SURVIVAL OF GLIOMA PATIENTS

A PREPRINT

Ahmad Chaddad^{1,4*}, Paul Daniel², Mingli Zhang⁵, Saima Rathore⁶, Paul Sargos⁴, Christian Desrosiers³,
Tamim Niazi⁴

¹ School of Artificial intelligence, Guilin University of Electronic Technology, China

² Hudson Institute of Medical Research, Australia

³ The Laboratory for Imagery, Vision and Artificial Intelligence, Canada

⁴ Lady Davis Institute for Medical Research, McGill University, Canada

⁵ Montreal Neurological Institute, McGill University, Canada

⁶ Perelman School of Medicine, University of Pennsylvania, USA

email:ahmad8chaddad@gmail.com, ahmadchaddad@guet.edu.cn

June 10, 2022

ABSTRACT

Imaging biomarkers offer a non-invasive way to predict the response of immunotherapy prior to treatment. In this work, we propose a novel type of deep radiomic features (DRFs) computed from a convolutional neural network (CNN), which capture tumor characteristics related to immune cell markers and overall survival. Our study uses four MRI sequences (T1-weighted, T1-weighted post-contrast, T2-weighted and FLAIR) with corresponding immune cell markers of 151 patients with brain tumor. The proposed method extracts a total of 180 DRFs by aggregating the activation maps of a pre-trained 3D-CNN within labeled tumor regions of MRI scans. These features offer a compact, yet powerful representation of regional texture encoding tissue heterogeneity. A comprehensive set of experiments is performed to assess the relationship between the proposed DRFs and immune cell markers, and measure their association with overall survival. Results show a high correlation between DRFs and various markers, as well as significant differences between patients grouped based on these markers. Moreover, combining DRFs, clinical features and immune cell markers as input to a random forest classifier helps discriminate between short and long survival outcomes, with AUC of 72% and $p=2.36 \times 10^{-5}$. These results demonstrate the usefulness of proposed DRFs as non-invasive biomarker for predicting treatment response in patients with brain tumors.

1 Introduction

Gliomas are the most common tumors initiating in the brain. As defined by the World Health Organization (WHO) [1], gliomas can be classified into four grades (I, II, III or IV) by histopathological process depending on their aggressiveness. Grade I glioma represents non-invasive tumors, grade II/III corresponds to low/intermediate-grade gliomas also named lower grade glioma (LGG), and grade IV to aggressive malignant tumors called glioblastoma multiforme (GBM). GBM is the most deadly brain tumor with a median survival of 15 months [2]. Most patients relapse within months, after which there are limited options for further treatment. Immunotherapy is a promising strategy for cancer treatment in which the patient's own immune system is used to eliminate cancer cells [3]. Despite encouraging developments, predicting response to immunotherapy prior to treatment remains a challenging task for clinicians.

Intratumoral immune response was shown to be related to tumor progression and prognosis in gliomas [4, 5, 6]. Various markers, such as the CD3 (cluster of differentiation 3) marker, were investigated for evaluating intratumoral immune response. CD3 is a protein complex composed of CD3G, CD3D, and CD3E chains that is considered a general marker of T-cells. Antitumor immune responses have been correlated with clinical response to the immune therapeutic [7], with tumor-infiltrating CD3 T-cells and dendritic cell therapy for GBM patients [8]. Despite the high potential of

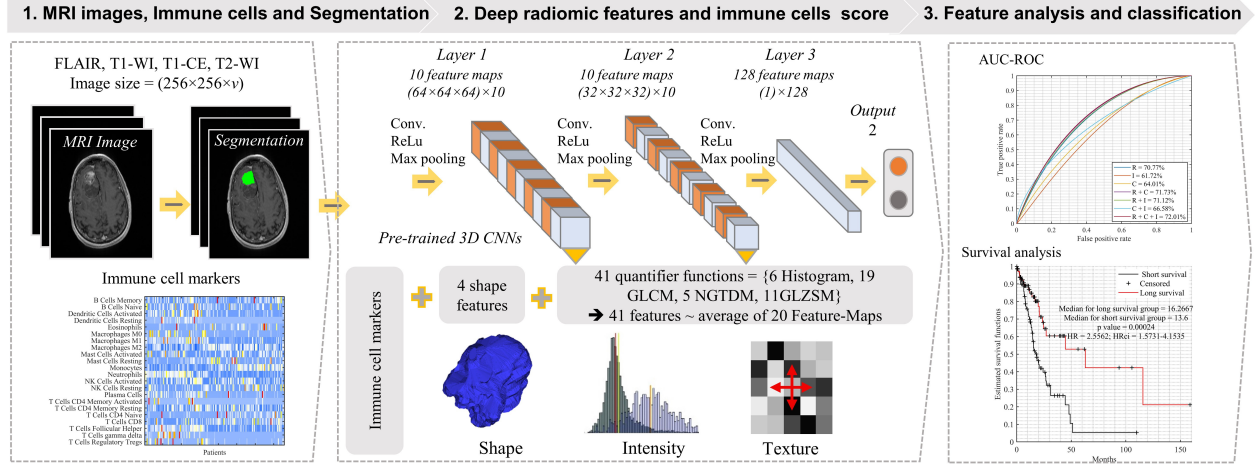


Figure 1: Deep radiomic pipeline for predicting immune cell markers and survival. 1) Image acquisition with manually segmented tumor masks. 2) Deep image feature extraction. 3) Predictive models and informatics analysis.

immunotherapy, the prediction of response to immune therapeutics usually requires an invasive technique by either biopsy or surgery, which is costly and has inherent risks of complications. Hence, the development of reliable imaging biomarkers that can capture characteristics of immune cells would provide a non-invasive alternative for improving the immune therapeutics process.

Recent work has examined the relationships between tumor imaging features (e.g., shape, texture, histogram), multi-omics (e.g., genomics, proteomics, transcriptomics) and clinical outcome [9, 10, 11]. Radiomics is a computational approach that seeks to convert medical images into quantitative data [12]. It has shown the ability to capture characteristics of tissue heterogeneity that are related to cellular and molecular properties [13, 14, 15]. Radiomic methods are typically used to derive image biomarkers for computer-aided diagnosis (CAD), and to monitor patients in pre- and post-treatment. Investigating the link between radiomic features and intratumoral immune response may thus provide a non-invasive technique for evaluating the benefit of immune therapeutics in individual patients [16]. In a recent study [17], a structured approach is provided to decipher tumor characteristics and its immune environment. Further, the usefulness of radiomic signatures has been demonstrated in estimating CD8 cell count and predicting clinical outcomes of patients treated with immunotherapy [18]. Another study [19] presents available immunotherapy regimens for evaluating the anti-tumor and immune responses to immunotherapy in neuro-oncology applications. The ratio of tumor volume in T2-FLAIR scans relative to the volume of contrast enhancement was shown to be associated to outcome for the mesenchymal subtype of GBM [20] which has a stronger immunological response compared to other GBM subtypes [21].

So far, no investigation has explored the potential of radiomic analysis to predict immune cell response and its impact on survival outcome for patients with LGG and GBM. To bridge this gap, we propose a novel radiomic signature for LGG and GBM brain tumors, based on the activation maps of a pre-trained 3D convolutional neural network (CNN). Our model extends the work in [22, 32, 37], where the entropy of CNN activations was considered as measure of texture heterogeneity, and proposes a broader set of CNN-based features which capture important characteristics of tumor heterogeneity that are related to immune cell markers. Specifically, the major contributions of this work are as follows:

- To our knowledge, this work is the first to encode CNN activation maps with standard radiomic functions for survival and immune cell marker prediction. The proposed Deep Radiomic Features (DRFs) offer a compact representation of image texture, which captures the heterogeneity of glioma tissues at different image scales.
- We present a detailed evaluation of the proposed DRFs on one of the largest publicly-available brain tumor datasets. Our results show their relationship to several immune cell markers and to overall patient survival. When used as input to a random forest classifier, our DRFs lead to a significantly higher accuracy than clinical features and immune cell markers for predicting shorter versus longer survival groups.

The rest of this paper is structured as follows. Section II describes the image data, clinical and immune cell markers, proposed deep radiomic features for predicting the immune cell scores and clinical outcomes of glioma patients. Section III provides experimental setup and results. Section IV discusses our findings. Finally, Section 5 concludes with a summary of our work’s main contributions and results.

2 Materials and methods

Figure 1 shows the pipeline of the proposed deep radiomic model. Four MRI sequences (T1-WI, T1-CE, FLAIR and T2WI) are first acquired. Segmentation is then performed by labelling the tumor regions of interest (ROIs) in each scan. Thereafter, DRFs are extracted from 3D CNN activations corresponding to segmented ROIs. Finally, statistical and classification analyses are conducted to assess the relationship between DRFs and immune cell markers and the DRFs' ability to predict the survival of glioma patients. The following subsections present each of these steps in greater detail.

2.1 Patient selection and image preprocessing

For this study, we used pre-surgical images and immune cell markers data from 151 patients in the TCGA database with histologically confirmed LGG or GBM. Patients were selected based on the availability of high-quality T1-weighted (T1-WI), T1-weighted post-contrast (T1-CE), T2-weighted (T2-WI) and FLAIR images associated with corresponding immune cell markers and clinical information (age, gender and overall survival). Other patients with imaging data are available, however have unclear tumor regions in corresponding MRI sequences and/or no immune cell markers, which are required for the prediction tasks of this study.

Images for these 151 patients were obtained from The Cancer Imaging Archive (TCIA) [26]. Patients have been previously de-identified by TCGA/TCIA, and no institutional review board or Health Insurance Portability and Accountability Act approval were required for our study. Note that the TCGA/TCIA scans were obtained from multiple sites, and thus the scanner model, pixel spacing, slice thickness and contrast varies within the selected cohort. We considered these differences by sampling all volumes to a common voxel resolution of 1 mm^3 with a total size of $256 \times 256 \times \text{slices}$ voxels. Additionally, intensities in each volume were normalised to the $[0, 1]$ range. Immune cell markers ($n=22$) are the immune cellular fraction that was estimated using CIBERSORT [25]. These proportions were multiplied by leukocyte fraction to yield corresponding estimates in terms of overall fraction in tissue. More details on these markers are reported in [7]. Demographic information of the study population can be found in Table 1.

2.2 Segmentation

Tumors were labeled semi-automatically using the 3D Slicer software 3.6¹. ROIs were determined separately by two expert oncologists, slice by slice from axial images under blind conditions. Those ROIs (contours) were then interpolated to obtain the 3D volumetric tumor mask. The same segmentation procedure was applied to all MRI sequences.

2.3 Proposed deep imaging features

Convolutional neural networks (CNNs) are widely used in medical image analysis and have achieved state-of-art performance for various image classification tasks, in particular when large sets of images are available [27, 28]. Typical CNN architectures are comprised of a repeated stack of convolution and pooling layers, followed by one or more fully-connected layers [29]. Convolution layers have a filtering function extracting spatial features from the image. While initial layers capture local image patterns, deep layers extract high-level features representing global structure and texture. To add non linearity, non-saturating activation functions such as the Rectified Linear Unit (ReLU) [30] are typically used instead of more traditional functions like the sigmoid. Functions like the ReLU help alleviate the vanishing gradient problem when training deep networks with gradient descent in deep networks. Pooling layers (e.g., maximum or average) are typically added after each convolution layer block to reduce the spatial dimension of activation maps and make the network invariant to small image translations. CNNs for classification also have fully-connected layers followed by an output layer (e.g., Softmax) which converts logits into class probabilities. During training, convolutional filters and fully-connected layer weights are updated using the backpropagation algorithm.

Inspired by studies exploring the flow of information in deep neural networks [23, 24, 34, 35], the entropy of CNN activation maps was proposed as a compact description of texture in medical images [22, 32, 37]. Although these entropy-based features were shown to be predictive of different diseases, they only offer a limited measure of heterogeneity and do not capture the full range of statistics describing the texture of affected tissues. To overcome this limitation, we derive a richer set of texture features from CNN activations. Toward this goal, deep texture features are extracted from a pre-trained 3D CNN architecture which was previously used in [37]. This network was trained on multi-site 3D MRI data for binary classification of Alzheimer's using cross entropy loss, as well as stochastic gradient descent optimization with a momentum of 0.9 and learning rate of 0.0005. We generated texture descriptors from gross total

¹<http://www.slicer.org/>

resection (tumor ROI) using the pre-trained 3D CNN and encoded the activation maps ($n=20$) in layer 1 and layer 2, respectively, by applying the following 41 quantifier functions:

- **Histogram:** mean, variance, skewness, kurtosis, energy and entropy;
- **Texture:** grey level co-occurrence matrix (GLCM) [38], neighborhood gray-tone difference matrix (NGTDM) [39] and gray-level zone size matrix (GLSZM) [40]. Image intensities of volumetric tumor/ROIs were uniformly resampled to 32 grey-levels before computation to capture more meaningful texture patterns.

The detailed definition of these descriptor functions/features is provided in the supplementary materials of [9]. Descriptors derived from the 20 activation maps were averaged and combined with 4 shape features (porosity, fraction dimension, surface-area and volume) to obtain a set of 45 features. Applying this procedure for each image modality (i.e., T1-WI, T1-CE, T2-WI and FLAIR) yielded a total of 180 DRFs (45 features for each of the four modalities).

Table 1: Demographic information of the study population.

		TCGA/TCIA ($n=151$)
Gender	Male	86
	Female	65
Grade	LGG	83
	GBM	68
Age	Median (min-max)	53 (19-84.8)
	Average	51.34
Survival	Median (months)	14.43
	Dead (censored)	68 (83)
Immune cells (presence/absence)	B Cells Memory	102/49
	B Cells Naive	75/76
	Dendritic Cells Activated	74/77
	Dendritic Cells Resting	31/120
	Eosinophils	45/106
	Macrophages M0	43/108
	Macrophages M1	112/39
	Macrophages M2	151/0
	Mast Cells Activated	91/60
	Mast Cells Resting	63/88
	Monocytes	139/12
	Neutrophils	120/31
	NK Cells Activated	107/44
	NK Cells Resting	74/77
	Plasma Cells	59/92
	T Cells CD4 Memory Activated	12/139
	T Cells CD4 Memory Resting	135/16
	T Cells CD4 Naive	47/104
	T Cells CD8	111/40
	T Cells Follicular Helper	132/19
	T Cells gamma delta	29/122
	T Cells Regulatory Tregs	34/117

2.4 Statistical and survival analysis

Features analysis Spearman rank correlation (ρ) was used to measure the relationship between pairs of features (e.g., DRF and immune cell markers), and the Wilcoxon test to compare between two groups with continuous variables (e.g., low vs. high immune cell markers) [41]. To account for multiple comparisons, all p-values obtained from significance testing were simultaneously corrected according to the Holm-Bonferroni method [42]. A threshold of $p < 0.05$ on corrected p-values was used to identify statistically significant features.

Survival analysis The log-rank test [43] was used to compare between the lower-than-median and higher-than-median survival groups of patients for each feature. We considered the survival as the number of days to death (i.e.,

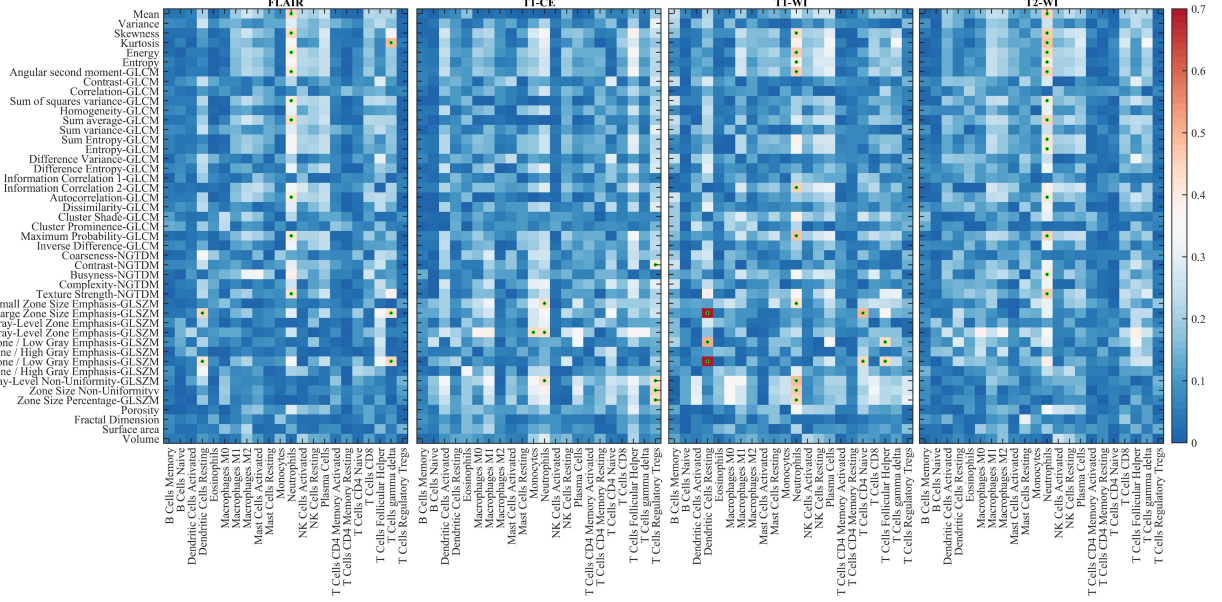


Figure 2: Heatmap of Spearman correlation value between immune cell markers and DRFs. Green circles represent the significant features following Holm-Bonferroni with $p < 0.05$.

sensorship=1) for deceased patients, or days to last visit or follow up (i.e., sensorship=0) since initial diagnostic otherwise. Once again, differences were considered statistically significant if $p < 0.05$ after correction.

Classification We used the area under the receiver operator characteristic curve (AUC) to assess whether the DRF signature could classify low from high immune cell markers, and separate patients into short and long survival groups. Specifically, we used all the DRFs as the input of the random forest (RF) classifier to classify between two groups of patients (below vs above median value of immune cell marker; shorter vs longer survival groups using the median survival as cut-off). Note that different classifiers could have been considered for this task, however we chose the RF model since it is recommended when training data is limited and it can be used to inspect predictive features that are most important in classification [44]. To train the RF model for classifying between shorter and longer survival groups, we applied an imputation technique to censored patients, for which only a lower bound on survival is known. Specifically, censored patients were assigned the average survival of uncensored subjects with a time-to-death greater or equal to their own time of last visit.

We considered two strategies for measuring the AUC [45]: 1) Leave-one-out cross validation (LOOCV) where training images are divided into n samples and, at each iteration, a single sample is put aside for testing and the remaining $n - 1$ samples are used to train the RF classifier. The final reported AUC is the mean over n iterations. 2) Single split, where we divide samples randomly into training ($n=100$) and testing ($n=51$) set, train the RF model using the training samples and test the model using the test samples. The reported AUC value is computed on the set of test samples. All our processing/analysis steps were performed using Matlab's Statistics and Machine Learning Toolbox.

3 Results

3.1 Feature related to immune cell markers

For brain tumor patients in the training set ($n=100$), the analysis on Spearman correlation shows that Dendritic-cells-activated (FLAIR and T1-WI), Neutrophils (FLAIR, T1-CE, T1-WI and T2-WI), T-cells-CD8 (FLAIR, and T1-WI), T-Cells-CD4-Naïve (T1-WI) and T-Cells-Regulatory-Tregs (T1-CE) are significantly correlated to DRFs with an absolute value in the range of 0.4-0.74 and corrected $p < 0.05$. Dendritic-cells-activated has the highest absolute correlation of 0.74 with DRFs derived T1-WI (Large Zone Size Emphasis-GLSZM and Large Zone / Low Gray Emphasis-GLSZM) (Figure 2).

We then sought to investigate whether individual DRFs could predict immune cell markers. Toward this goal, patients were divided in two groups using the median value of each immune cell markers, i.e. less than median value vs.

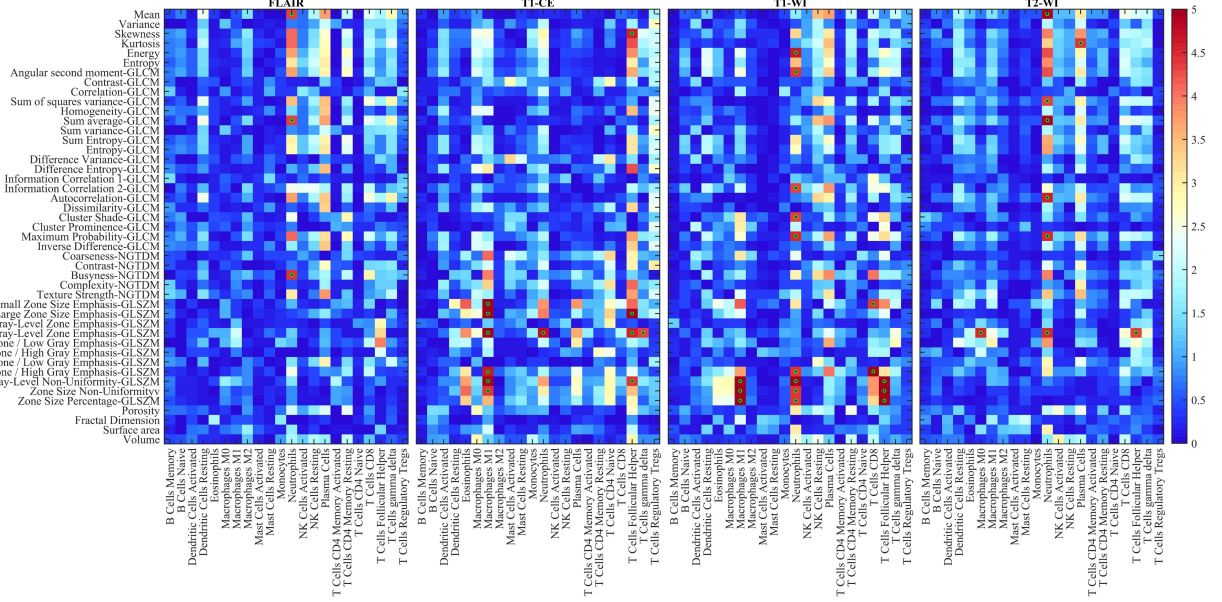


Figure 3: Heatmap of significance value ($-\log_{10}(\text{p-value})$) using the Wilcoxon test to compare DRFs between low and high scores of immune cell markers. Green circles represent the significant features following Holm-Bonferroni with $p < 0.05$.

greater than median value. The ability of each DRF to predict immune cell markers was then evaluated using Wilcoxon significance testing (Figure 3). We see that DRFs are able to discriminate between low and high groups of Neutrophils score (FLAIR, T1-CE, T1-WI and T2-WI), Macrophage-M0 (T2-WI), Macrophage-M1 (T1-CE and T1-WI), T-Cells-Follicular-Helper (T1-CE, T1-WI and T2-WI) and T-Cells-gamma-delta (T1-CE) with corrected $p < 0.05$. Highest significance values are obtained while using DRFs extracted from T1-WI (Gray-Level-Non-Uniformity-GLSZM, Zone Size Non-Uniformity and Zone Size Percentage-GLSZM) to compare between low and high scores of Neutrophils, Macrophage-M1 and T-Cells-Follicular-Helper status, respectively.

Although a direct connection between DRFs and immune cell markers is hard to establish, their association may be explained by cellular characteristics of glioma which affect both the immune system's response and the tumor's appearance in MRI scans. These subtle differences in regional texture can be captured effectively by specifically designed descriptors such as those used in our work.

3.2 DRFs, clinical and immune cell markers related to survival

We next evaluate whether individual features from the set of 45 DRFs, 2 clinical (age and gender) and 22 immune cells features can predict patient survival. For this analysis, we performed a significance test on the same training set of patients with brain tumors ($n=100$). Except for gender, we grouped patients using the median value of each feature (45 DRFs, age, and immune cell markers) to separate patients into groups corresponding to greater vs. less than median feature value. The log-rank significance test was employed to compare between these two groups. We find that age, Macrophages M1, T Cells CD4 Naïve, Neutrophils, T Cells Follicular Helper and 50 DRFs are significantly associated with survival outcome, with the most significant clinical, DRFs and immune cell markers being age, information correlation derived from T1-WI and Macrophage M1, respectively (Table 2). Results for all features are reported in Table 2S of supplementary materials.

3.3 Building radiomic signature related to survival

We employed the RF model inside LOOCV to classify the 151 patients in the shorter-term or longer-term survival group using the 180 DRFs (R), 2 clinical features (C), 22 immune cell markers (I) features, or the combination of different feature types (R+I, R+C or R+C+I). Considering individually each type of feature, we see that DRFs give the highest accuracy, with an AUC of 70.77% compared to 64.01% for clinical features and 61.72% for immune cell markers (Figure 4a). Moreover, a significant improvement is achieved when combining both clinical features and immune markers with DRFs, with a highest AUC of 72.01% when using all features as input to the RF model

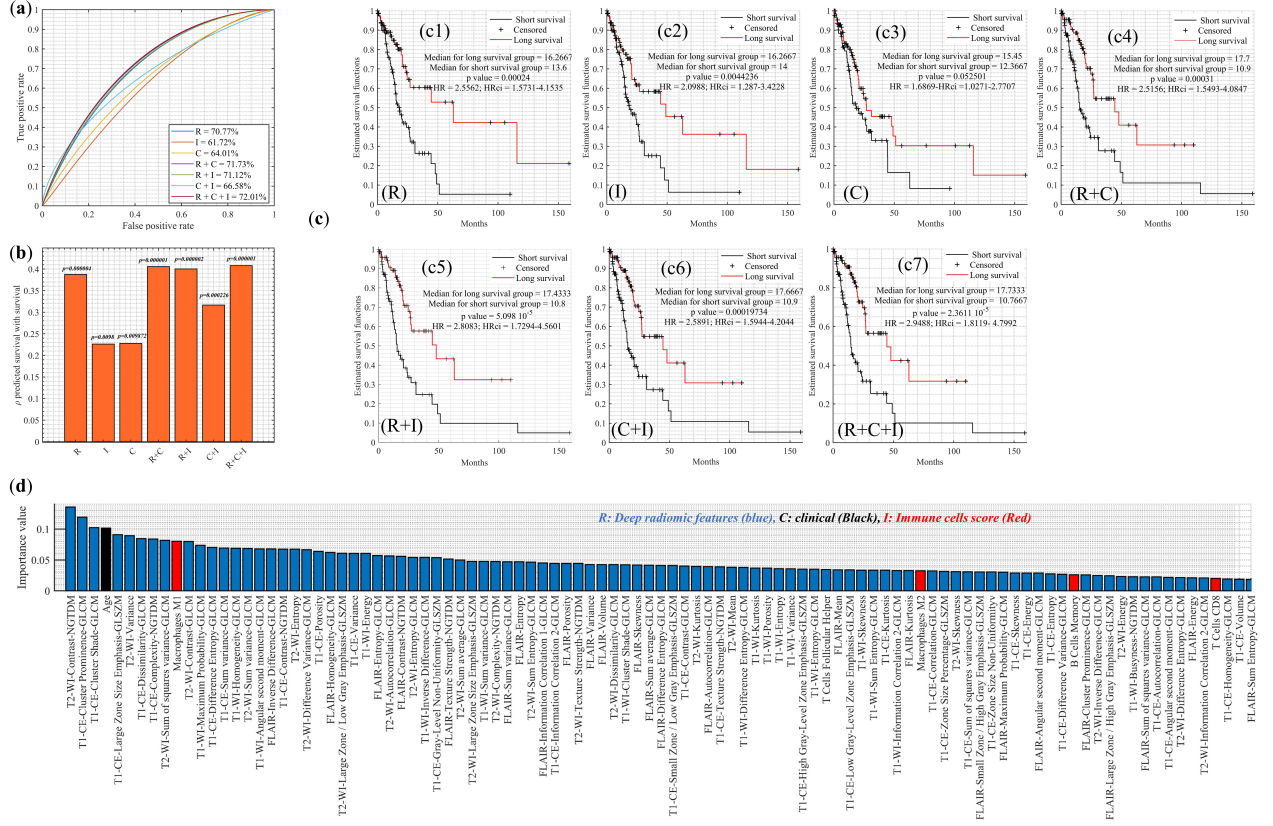


Figure 4: Predicting the survival outcome of 151 patients with brain tumors (LGG+GBM). (a) AUC-ROC values using 180 DRFs/radiomic features (R), 2 clinical (C) and 22 immune cell markers (I) and their combinations (R+C, R+I, C+I and R+C+I). (b) Bars represent the Spearman correlation between predicted short and long survival score and their corresponding survival. (c) Log-rank and Kaplan-Meier estimator (c1-c7) to compare survival between two predicted survival groups based on RF models. (d) Importance value of top 100 combined features (R+C+I) from a total 204 features.

(R+C+I). Measuring the Spearman correlation (ρ) between the score predicted by the RF model and the survival of the 151 patients (Figure 4b), we obtain an absolute correlation of 0.23-0.43 with corrected $p < 0.05$. Figure 4c shows results of the log-rank significance test and Kaplan-Meier estimator to assess our combined models' ability to predict survival. We observe that differential survival can be predicted when considering the following feature combinations: R ($p=0.0002$, HR=2.5, CI=1.5-4.1), I ($p=0.004$, HR=2.09, CI=1.28-3.4), R+C ($p=0.0003$, HR=2.51, CI=1.54-4.08), R+I ($p=5.09 \times 10^{-5}$, HR=2.8, CI=1.72-4.56), C+I ($p=1.9 \times 10^{-4}$, HR=2.5, CI=1.59-4.2) and R+C+I ($p=2.36 \times 10^{-5}$, HR=2.94, CI=1.81-4.79). We note that combined age and gender features do not lead to statistical significance. Among the 214 features (i.e., 180 DRFs + 22 immune cell markers + 2 clinical), we find 154 features predictive of survival in brain tumor patients (Figure 4d). Specifically, the Contrast-NGTDM from T2-WI, age, and macrophage M1 are the highest predictive features from DRFs, clinical features and immune cell markers, respectively. The Neighbouring Gray Tone Difference Matrix (NGTDM) measures the difference between a gray value and the average gray value of its neighbours within a given distance. A high NGTDM contrast occurs in tumor regions with a large range of gray levels and significant changes in intensity between voxels and their neighbourhood. The importance values of all R+I+C features for predicting survival are reported in Table 4S.

3.4 Radiomic signature predicts immune cells status

We used the 180 DRFs as input to the RF model from predicting lower and higher values of immune markers, with the LOOCV on the whole set of patients ($n=151$) or with a single training/testing split ($n=100/51$). Results in Figure 5 show high AUC values ($>80\%$) for Macrophage M1 (T1-CE), Neutrophils (T1-WI and FLAIR) and T Cells Follicular Helper (T2-WI). These findings are observed for both the LOOCV and training-testing split, with the highest AUC value of 84.81% obtained while using T1-WI DRFs to predict lower or higher values for the neutrophils marker. Figure

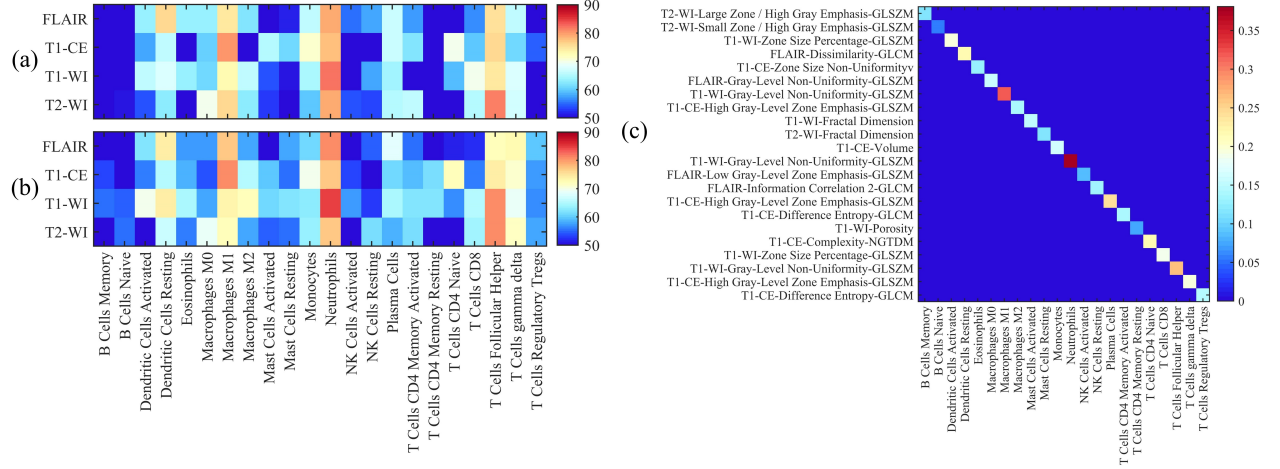


Figure 5: Heatmap of AUC value obtained in predicting low from a high score of 22 immune cell markers using the RF models in (a) LOOCV with 100 samples and (b) training/testing of 100/51 samples. (c) Heatmap of the highest predictive feature for each of the 22 immune cell markers.

5c shows the most important features for discriminating between lower and higher values of each of the 22 immune cell markers. We see that Gray-level-non-uniformity is the most predictive feature for Neutrophils, Macrophage M1 and T cells Follicular Helper markers. Results for all features and cell markers are reported in Table 5S.

4 Discussion

The prediction of immune status may help identify cancer patients that will respond to treatment [46]. Radiomics is a non-invasive technique for the automated prognosis of various types of tumors which uses a wide range of imaging features extracted from a region of interest (ROI) [47, 48]. While standard radiomic features have shown promising results [9, 13, 16, 18, 49], the use of multiscale features from different 3D CNN layers as learnable radiomics descriptors remains limited [37]. Using these deep features in combination with clinical variables and immune cell markers could improve the prediction of treatment response, thereby enabling the selection of optimal treatment for individual patients. Toward this goal, we proposed a novel radiomic analysis pipeline that considers 41 descriptors extracted from 3D CNN activation maps to predict survival and the value of immune cell markers.

Our study showed that DRFs derived from a pre-trained 3D CNN can accurately predict the survival group of patients as well as the low or high value of immune cell markers. In our experiments, the combination of DRFs, clinical features and immune cell markers achieved the highest AUC of 72.01% (corrected $p < 0.05$) for classifying patients in groups corresponding to shorter (i.e., below median) or longer (i.e., above median) survival. The most predictive features in the RF model were found to be DRFs, age and Macrophage M1 (Figure 4). This result is consistent with previous work in the literature which showed age [50, 51], Macrophage [7, 52] and radiomic features to be associated with survival outcome [49, 53, 54, 55]. The proposed analysis also shown that combined DRFs give the highest accuracy to predict the low or high value of Macrophage-M1, Neutrophils and T-cells-follicular-helper immune cell markers with an AUC $> 80\%$. Moreover, the gray-level non uniformity descriptor derived from T1-WI images was the most predictive feature for these three immune cell markers (Figure 5). This confirms the potential of radiomic features for predicting immune markers [49, 56, 57].

By incorporating immune cell markers in the proposed method, this study aims to enhance the impact of immunotherapy in clinical practice. This is similar to the recent work in [16] which presented a radiomics approach to predict the response to cancer immunotherapy. Our study is also related to radiogenomics profiling methods to identify MRI-associated immune cell markers in GBM which are correlated with prognosis. For instance, CD49d expression level was found to be correlated with apparent diffusion coefficient (ADC) and shown to be a useful biomarker to predict progression of GBM patients [58]. Likewise, the reduction in the tumor-promoting effects of monocytes/macrophages in GBM was considered as an adjuvant treatment for glioma [59]. It was demonstrated that determining the various roles of immune cell markers has an impact on the diagnosis and prediction of cancer progression [60] and recurrent GBM [61, 62].

Table 2: List of 55 significant features to compare between survival of patient grouped by individual feature values.

Features (DRFs, clinical, immune cells)	Median survival		P-value	HR	Confidence interval		Corrected p-value
	\geq	$<$			CI1	CI2	
Age	10.6	17.0	5.45×10^{-8}	4.16	2.52	6.87	0.00001
T1-WI-Information Correlation 2-GLCM	17.2	11.4	3.88×10^{-7}	0.27	0.16	0.44	0.00008
T1-WI-Maximum Probability-GLCM	11.0	17.7	1.36×10^{-6}	3.51	2.14	5.76	0.00028
Macrophages M1	13.3	15.5	1.40×10^{-6}	3.40	2.09	5.52	0.00028
T2-WI-Sum of squares variance-GLCM	17.1	11.8	2.00×10^{-6}	0.30	0.18	0.48	0.00040
T2-WI-Autocorrelation-GLCM	17.1	11.8	2.00×10^{-6}	0.30	0.18	0.48	0.00040
T2-WI-Sum variance-GLCM	17.1	11.4	2.09×10^{-6}	0.28	0.17	0.47	0.00041
T2-WI-Energy	11.0	18.6	3.63×10^{-6}	3.30	2.02	5.40	0.00072
T2-WI-Variance	16.3	11.8	4.18×10^{-6}	0.30	0.18	0.49	0.00082
T1-WI-Skewness	11.9	17.4	4.42×10^{-6}	3.28	2.00	5.36	0.00086
T1-WI-Energy	11.0	17.7	6.69×10^{-6}	3.18	1.95	5.20	0.00130
T2-WI-Entropy-GLCM	18.4	11.4	6.80×10^{-6}	0.31	0.19	0.51	0.00131
T1-CE-Large Zone Size Emphasis-GLSZM	15.4	13.1	7.49×10^{-6}	0.32	0.19	0.52	0.00144
T2-WI-Entropy	18.4	11.4	8.02×10^{-6}	0.32	0.19	0.52	0.00153
T2-WI-Porosity	11.0	18.4	8.23×10^{-6}	3.17	1.93	5.18	0.00156
T1-WI-Gray-Level Non-Uniformity-GLSZM	14.1	14.6	8.43×10^{-6}	3.07	1.90	4.97	0.00159
T1-WI-Angular second moment-GLCM	11.0	17.7	8.64×10^{-6}	3.14	1.92	5.12	0.00162
T2-WI-Mean	17.1	11.8	8.81×10^{-6}	0.32	0.20	0.52	0.00165
T2-WI-Sum average-GLCM	17.1	11.8	8.81×10^{-6}	0.32	0.20	0.52	0.00165
T2-WI-Small Zone / Low Gray Emphasis-GLSZM	12.2	16.0	8.91×10^{-6}	3.20	1.94	5.28	0.00165
T2-WI-Skewness	11.0	17.4	9.28×10^{-6}	3.11	1.91	5.08	0.00171
T1-CE-Kurtosis	15.1	14.1	9.37×10^{-6}	0.32	0.20	0.52	0.00172
T2-WI-Kurtosis	11.0	17.2	9.70×10^{-6}	3.08	1.90	5.00	0.00177
T2-WI-Contrast-NGTDM	16.3	12.0	1.02×10^{-5}	0.32	0.20	0.52	0.00184
T2-WI-Sum Entropy-GLCM	18.4	11.4	1.03×10^{-5}	0.32	0.20	0.53	0.00186
T1-WI-Entropy	17.7	11.8	1.48×10^{-5}	0.33	0.20	0.54	0.00266
T1-CE-Dissimilarity-GLCM	11.0	16.2	1.64×10^{-5}	3.08	1.87	5.07	0.00292
T2-WI-Contrast-GLCM	17.1	12.6	1.72×10^{-5}	0.33	0.20	0.54	0.00305
T1-CE-Complexity-NGTDM	11.0	15.5	1.89×10^{-5}	3.01	1.84	4.92	0.00332
T2-WI-Difference Variance-GLCM	16.3	12.1	1.95×10^{-5}	0.33	0.20	0.54	0.00340
T2-WI-Angular second moment-GLCM	11.9	17.7	2.23×10^{-5}	2.96	1.82	4.81	0.00388
T1-WI-Sum Entropy-GLCM	17.7	11.8	2.31×10^{-5}	0.34	0.21	0.55	0.00400
T1-CE-Skewness	15.1	14.0	3.30×10^{-5}	0.34	0.21	0.56	0.00567
T2-WI-Maximum Probability-GLCM	11.9	17.4	3.38×10^{-5}	2.88	1.77	4.68	0.00579
T2-WI-Volume	17.8	11.4	3.42×10^{-5}	0.35	0.21	0.56	0.00581
T2-WI-Large Zone / Low Gray Emphasis-GLSZM	11.7	17.7	5.80×10^{-5}	2.79	1.72	4.53	0.00980
T1-WI-Porosity	12.0	17.7	5.82×10^{-5}	2.83	1.73	4.64	0.00980
T1-CE-Gray-Level Non-Uniformity-GLSZM	11.7	15.4	6.84×10^{-5}	2.79	1.71	4.56	0.01142
T1-CE-Contrast-NGTDM	12.2	15.6	7.42×10^{-5}	2.80	1.71	4.58	0.01231
T1-WI-Small Zone Size Emphasis-GLSZM	14.1	14.6	8.14×10^{-5}	2.70	1.67	4.36	0.01343
FLAIR-Kurtosis	12.2	17.4	8.33×10^{-5}	2.71	1.67	4.39	0.01367
FLAIR-Difference Entropy-GLCM	16.8	11.4	1.10×10^{-4}	0.37	0.23	0.61	0.01791
T Cells CD4 Naive	15.3	13.6	1.21×10^{-4}	0.36	0.22	0.59	0.01963
T2-WI-Large Zone Size Emphasis-GLSZM	11.9	16.5	1.31×10^{-4}	2.67	1.64	4.34	0.02113
Neutrophils	14.7	13.1	1.46×10^{-4}	2.60	1.61	4.20	0.02338
FLAIR-Energy	12.2	16.9	1.49×10^{-4}	2.61	1.61	4.22	0.02376
FLAIR-Angular second moment-GLCM	12.2	16.9	1.59×10^{-4}	2.60	1.61	4.20	0.02511
FLAIR-Mean	17.1	12.1	1.61×10^{-4}	0.38	0.24	0.62	0.02532
FLAIR-Sum average-GLCM	17.1	12.1	1.61×10^{-4}	0.38	0.24	0.62	0.02532
T1-CE-Large Zone / High Gray Emphasis-GLSZM	15.7	12.0	1.75×10^{-4}	0.38	0.23	0.62	0.02719
FLAIR-Maximum Probability-GLCM	12.0	17.4	1.83×10^{-4}	2.59	1.60	4.19	0.02813
FLAIR-Texture Strength-NGTDM	11.7	16.5	2.06×10^{-4}	2.56	1.58	4.13	0.03156
T Cells Follicular Helper	12.2	15.2	2.61×10^{-4}	2.53	1.56	4.11	0.03969
FLAIR-Skewness	12.2	16.5	2.82×10^{-4}	2.50	1.55	4.04	0.04252
FLAIR-Sum Entropy-GLCM	17.7	11.4	3.23×10^{-4}	0.40	0.25	0.65	0.04844

Our findings suggest the proposed imaging features to be related to neutrophils, macrophage and follicular helper T-cells markers. Pre-treatment neutrophils can potentially serve as a prognostic marker in predicting the chemotherapeutic response and survival outcomes in glioma [63]. Macrophage and follicular helper T-cells were also demonstrated as immune therapeutic markers for glioma patients and were correlated with an unfavorable prognostic [64, 65, 66]. Moreover, radiomic signatures (i.e., imaging features) were shown to be related to tumor variations and changes in vascularization and inflammatory status [67, 68, 69]. However, a systematic biological approach such as an animal model is necessary to clarify and validate the relationship between immune cell markers and proposed imaging features.

Our study has some limitations worth of mention, such as the use of standard MR imaging sequence (T1-WI, T1-CE, FLAIR and T2-WI). Thus, considering ADC and dynamic contrast-enhanced (DCE) sequences with additional immune cell markers could improve our method's accuracy. Furthermore, validating our method on other datasets could further help demonstrate its usefulness to clinical practice.

5 Conclusion

This study investigated deep radiomic descriptors derived from 3D CNN features maps for predicting the immune cell makers and survival outcome in patients with brain tumors. Our findings suggest associations between deep features, immune cell markers and survival of patients with glioma. Our work provides a model that could potentially be used for accurately predicting three immune cell markers and the survival outcome of patients. Motivated by these results, we aim to expand the proposed deep radiomic pipeline across various cancer types.

References

- [1] R. Stupp et al., “Changing Paradigms—An Update on the Multidisciplinary Management of Malignant Glioma,” *The Oncologist*, vol. 11, no. 2, pp. 165–180, Feb. 2006.
- [2] E. M. Sizoo et al., “Measuring health-related quality of life in high-grade glioma patients at the end of life using a proxy-reported retrospective questionnaire,” *J. Neurooncol.*, vol. 116, no. 2, pp. 283–290, Jan. 2014.
- [3] N. F. Brown, T. J. Carter, D. Ottaviani, and P. Mulholland, “Harnessing the immune system in glioblastoma,” *Br. J. Cancer*, vol. 119, no. 10, pp. 1171–1181, 2018.
- [4] M. J. M. Gooden, G. H. de Bock, N. Leffers, T. Daemen, and H. W. Nijman, “The prognostic influence of tumor-infiltrating lymphocytes in cancer: a systematic review with meta-analysis,” *Br. J. Cancer*, vol. 105, no. 1, pp. 93–103, Jun. 2011.
- [5] A. B. Heimberger et al., “Incidence and prognostic impact of FoxP3+ regulatory T cells in human gliomas,” *Clin. Cancer Res.*, vol. 14, no. 16, pp. 5166–5172, Aug. 2008.
- [6] I. Yang et al., “CD8+ T-cell infiltrate in newly diagnosed glioblastoma is associated with long-term survival,” *J Clin Neurosci*, vol. 17, no. 11, pp. 1381–1385, Nov. 2010.
- [7] V. Thorsson et al., “The Immune Landscape of Cancer,” *Immunity*, vol. 48, no. 4, pp. 812–830.e14, 17 2018.
- [8] R. M. Prins et al., “Gene Expression Profile Correlates with T-Cell Infiltration and Relative Survival in Glioblastoma Patients Vaccinated with Dendritic Cell Immunotherapy,” *Clin Cancer Res*, vol. 17, no. 6, pp. 1603–1615, Mar. 2011.
- [9] A. Chaddad, P. Daniel, S. Sabri, C. Desrosiers, and B. Abdulkarim, “Integration of Radiomic and Multi-omic analyzes Predicts Survival of Newly Diagnosed IDH1 Wild-Type Glioblastoma,” *Cancers*, vol. 11, no. 8, p. 1148, Aug. 2019.
- [10] M. Zanfardino et al., “Bringing radiomics into a multi-omics framework for a comprehensive genotype–phenotype characterization of oncological diseases,” *Journal of Translational Medicine*, vol. 17, no. 1, p. 337, Oct. 2019.
- [11] D. Nie et al., “Multi-Channel 3D Deep Feature Learning for Survival Time Prediction of Brain Tumor Patients Using Multi-Modal Neuroimages,” *Scientific Reports*, vol. 9, no. 1, p. 1103, Jan. 2019.
- [12] E. J. Limkin et al., “Promises and challenges for the implementation of computational medical imaging (radiomics) in oncology,” *Ann. Oncol.*, vol. 28, no. 6, pp. 1191–1206, Jun. 2017.
- [13] A. Chaddad et al., “Radiomics in Glioblastoma: Current Status and Challenges Facing Clinical Implementation,” *Front Oncol*, vol. 9, May 2019.
- [14] P. P. Batchala et al., “Neuroimaging-Based Classification Algorithm for Predicting 1p/19q-Codeletion Status in IDH-Mutant Lower Grade Gliomas,” *American Journal of Neuroradiology*, vol. 40, no. 3, pp. 426–432, Mar. 2019.
- [15] H. Zhou et al., “Machine learning reveals multimodal MRI patterns predictive of isocitrate dehydrogenase and 1p/19q status in diffuse low- and high-grade gliomas,” *J Neurooncol*, vol. 142, no. 2, pp. 299–307, Apr. 2019.
- [16] S. Trebeschi et al., “Predicting Response to Cancer Immunotherapy using Non-invasive Radiomic Biomarkers,” *Ann. Oncol.*, Mar. 2019.
- [17] M. Sinigaglia et al., “Imaging-guided precision medicine in glioblastoma patients treated with immune checkpoint modulators: research trend and future directions in the field of imaging biomarkers and artificial intelligence,” *EJNMMI Res*, vol. 9, Aug. 2019.
- [18] R. Sun et al., “A radiomics approach to assess tumor-infiltrating CD8 cells and response to anti-PD-1 or anti-PD-L1 immunotherapy: an imaging biomarker, retrospective multicohort study,” *The Lancet Oncology*, vol. 19, no. 9, pp. 1180–1191, Sep. 2018.
- [19] B. B. Kasten et al., “Current and Future Imaging Methods for Evaluating Response to Immunotherapy in Neuro-Oncology,” *Theranostics*, vol. 9, no. 17, pp. 5085–5104, 2019.

- [20] K. M. Naeini et al., “Identifying the mesenchymal molecular subtype of glioblastoma using quantitative volumetric analysis of anatomic magnetic resonance images,” *Neuro-oncology*, vol. 15, no. 5, pp. 626–634, May 2013.
- [21] T. Doucette et al., “Immune heterogeneity of glioblastoma subtypes: extrapolation from the cancer genome atlas,” *Cancer Immunol Res*, vol. 1, no. 2, pp. 112–122, Aug. 2013.
- [22] A. Chaddad, M. Toews, C. Desrosiers, and T. Niazi, “Deep Radiomic Analysis Based on Modeling Information Flow in Convolutional Neural Networks,” *IEEE Access*, vol. 1, pp. 97242–97252, 2019.
- [23] N. Tishby and N. Zaslavsky, “Deep learning and the information bottleneck principle,” in *2015 IEEE Information Theory Workshop (ITW)*, 2015, pp. 1–5.
- [24] M. Gabri   et al., “Entropy and mutual information in models of deep neural networks,” in *Advances in Neural Information Processing Systems 31*, S. Bengio, H. Wallach, H. Larochelle, K. Grauman, N. Cesa-Bianchi, and R. Garnett, Eds. Curran Associates, Inc., 2018, pp. 1821–1831.
- [25] A. J. Gentles et al., “The prognostic landscape of genes and infiltrating immune cells across human cancers,” *Nature Medicine*, vol. 21, no. 8, pp. 938–945, Aug. 2015.
- [26] F. W. Prior et al., “TCIA: An information resource to enable open science,” *Conf Proc IEEE Eng Med Biol Soc*, vol. 2013, pp. 1282–1285, 2013.
- [27] G. Litjens et al., “A survey on deep learning in medical image analysis,” *Medical Image Analysis*, vol. 42, pp. 60–88, Dec. 2017.
- [28] S. L. Goldenberg, G. Nir, and S. E. Salcudean, “A new era: artificial intelligence and machine learning in prostate cancer,” *Nature Reviews Urology*, p. 1, May 2019.
- [29] F. Chollet, *Deep Learning mit Python und Keras: Das Praxis-Handbuch vom Entwickler der Keras-Bibliothek*. MITP-Verlags GmbH & Co. KG, 2018.
- [30] C. Nwankpa, W. Ijomah, A. Gachagan, and S. Marshall, “Activation Functions: Comparison of trends in Practice and Research for Deep Learning,” *arXiv preprint arXiv:1811.03378*, 2018.
- [31] N. Tishby, F. C. Pereira, and W. Bialek, “The information bottleneck method,” *arXiv:physics/0004057*, Apr. 2000.
- [32] A. Chaddad, C. Desrosiers, and T. Niazi, “Deep Radiomic Analysis of MRI Related to Alzheimer’s Disease,” *IEEE Access*, vol. 6, pp. 58213–58221, 2018.
- [33] J. P. W. Pluim, J. B. A. Maintz, and M. A. Viergever, “Mutual-information-based registration of medical images: a survey,” *IEEE Transactions on Medical Imaging*, vol. 22, no. 8, pp. 986–1004, Aug. 2003.
- [34] M. Chen and H. Jaenicke, “An Information-theoretic Framework for Visualization,” *IEEE Transactions on Visualization and Computer Graphics*, vol. 16, no. 6, pp. 1206–1215, Nov. 2010.
- [35] L. Xu, T. Lee, and H. Shen, “An Information-Theoretic Framework for Flow Visualization,” *IEEE Transactions on Visualization and Computer Graphics*, vol. 16, no. 6, pp. 1216–1224, Nov. 2010.
- [36] S. Yu, R. Jenssen, and J. C. Principe, “Understanding convolutional neural network training with information theory,” *arXiv preprint arXiv:1804.06537*, 2018.
- [37] A. Chaddad, M. Toews, C. Desrosiers, and T. Niazi, “Deep Radiomic Analysis Based on Modeling Information Flow in Convolutional Neural Networks,” *IEEE Access*, vol. 7, pp. 97242–97252, 2019.
- [38] R. M. Haralick, “Statistical and structural approaches to texture,” *Proceedings of the IEEE*, vol. 67, no. 5, pp. 786–804, May 1979.
- [39] M. Amadasun and R. King, “Textural features corresponding to textural properties,” *IEEE Transactions on Systems, Man and Cybernetics*, vol. 19, no. 5, pp. 1264–1274, Sep. 1989.
- [40] G. Thibault et al., “Texture indexes and gray level size zone matrix application to cell nuclei classification,” 2009.
- [41] J. W. Pratt, “Remarks on Zeros and Ties in the Wilcoxon Signed Rank Procedures,” *Journal of the American Statistical Association*, vol. 54, no. 287, pp. 655–667, 1959.
- [42] S. Holm, “A simple sequentially rejective multiple test procedure,” *Scandinavian journal of statistics*, pp. 65–70, 1979.
- [43] D. G. Kleinbaum and M. Klein, “Kaplan-Meier Survival Curves and the Log-Rank Test,” in *Survival Analysis*, Springer New York, 2012, pp. 55–96.
- [44] L. Breiman, “Random Forests,” *Machine Learning*, vol. 45, no. 1, pp. 5–32, Oct. 2001.
- [45] J. A. Hanley and B. J. McNeil, “The meaning and use of the area under a receiver operating characteristic (ROC) curve,” *Radiology*, vol. 143, no. 1, pp. 29–36, Apr. 1982.

- [46] P. S. Hegde, V. Karanikas, and S. Evers, “The Where, the When, and the How of Immune Monitoring for Cancer Immunotherapies in the Era of Checkpoint Inhibition,” *Clin Cancer Res*, vol. 22, no. 8, pp. 1865–1874, Apr. 2016.
- [47] A. Chaddad, P. Daniel, C. Desrosiers, M. Toews, and B. Abdulkarim, “Novel Radiomic Features Based on Joint Intensity Matrices for Predicting Glioblastoma Patient Survival Time,” *IEEE Journal of Biomedical and Health Informatics*, vol. 23, no. 2, pp. 795–804, Mar. 2019.
- [48] S. Rathore et al., “Radiomic MRI signature reveals three distinct subtypes of glioblastoma with different clinical and molecular characteristics, offering prognostic value beyond IDH1,” *Scientific Reports*, vol. 8, no. 1, p. 5087, Mar. 2018.
- [49] A. Bhatia et al., “MRI radiomic features are associated with survival in melanoma brain metastases treated with immune checkpoint inhibitors,” *Neuro-oncology*, Oct. 2019.
- [50] L. Sun, S. Zhang, H. Chen, and L. Luo, “Brain Tumor Segmentation and Survival Prediction Using Multimodal MRI Scans With Deep Learning,” *Front. Neurosci.*, vol. 13, 2019.
- [51] A. A. Alattar et al., “Prognostic Importance of Age, Tumor Location, and Tumor Grade in Grade II Astrocytomas: An Integrated Analysis of the Cancer Genome Atlas and the Surveillance, Epidemiology, and End Results Database,” *World Neurosurgery*, vol. 121, pp. e411–e418, Jan. 2019.
- [52] M. Gjorgjevski et al., “Molecular profiling of the tumor microenvironment in glioblastoma patients: correlation of microglia/macrophage polarization state with metalloprotease expression profiles and survival,” *Biosci Rep*, vol. 39, no. 6, Jun. 2019.
- [53] O. Morin et al., “Integrated models incorporating radiologic and radiomic features predict meningioma grade, local failure, and overall survival,” *Neuro Oncol Adv*, vol. 1, no. 1, May 2019.
- [54] P. Sanghani, A. B. Ti, N. K. Kam King, and H. Ren, “Evaluation of tumor shape features for overall survival prognosis in glioblastoma multiforme patients,” *Surgical Oncology*, vol. 29, pp. 178–183, Jun. 2019.
- [55] T. Sasaki et al., “Radiomics and MGMT promoter methylation for prognostication of newly diagnosed glioblastoma,” *Sci Rep*, vol. 9, no. 1, pp. 1–9, Oct. 2019.
- [56] C. A. McIntyre et al., “Abstract 2444: The use of CT radiomics to predict immune infiltrate in pancreatic ductal adenocarcinoma,” *Cancer Res*, vol. 79, no. 13 Supplement, pp. 2444–2444, Jul. 2019.
- [57] M. Ligerio et al., “1176O Artificial intelligence combining radiomics and clinical data for predicting response to immunotherapy,” *Ann Oncol*, vol. 30, no. Supplement 5, Oct. 2019.
- [58] H. R. Cho, H. Jeon, C.-K. Park, S.-H. Park, and S. H. Choi, “Radiogenomics Profiling for Glioblastoma-related Immune Cells Reveals CD49d Expression Correlation with MRI parameters and Prognosis,” *Sci Rep*, vol. 8, no. 1, pp. 1–11, Oct. 2018.
- [59] X. Feng et al., “Loss of CX3CR1 increases accumulation of inflammatory monocytes and promotes gliomagenesis,” *Oncotarget*, vol. 6, no. 17, pp. 15077–15094, Jun. 2015.
- [60] D. F. Quail and J. A. Joyce, “Microenvironmental regulation of tumor progression and metastasis,” *Nat. Med.*, vol. 19, no. 11, pp. 1423–1437, Nov. 2013.
- [61] S. Wang et al., “Multiparametric magnetic resonance imaging in the assessment of anti-EGFRvIII chimeric antigen receptor T cell therapy in patients with recurrent glioblastoma,” *Br J Cancer*, vol. 120, no. 1, pp. 54–56, Jan. 2019.
- [62] J. A. Wilcox, R. Ramakrishna, and R. Magge, “Immunotherapy in Glioblastoma,” *World Neurosurgery*, vol. 116, pp. 518–528, Aug. 2018.
- [63] Z. Wang, L. Zhong, G. Li, R. Huang, Q. Wang, Z. Wang, C. Zhang, B. Chen, T. Jiang, W. Zhang, Pre-treatment neutrophils count as a prognostic marker to predict chemotherapeutic response and survival outcomes in glioma: a single-center analysis of 288 cases, *Am J Transl Res*. 12 90–104.2020.
- [64] Y. Pires-Afonso, S.P. Niclou, A. Michelucci, Revealing and Harnessing tumor-Associated Microglia/Macrophage Heterogeneity in Glioblastoma, *Int J Mol Sci*. 21 .2020.
- [65] M.D. Sørensen, R.H. Dahlrot, H.B. Boldt, S. Hansen, B.W. Kristensen, tumor-associated microglia/macrophages predict poor prognosis in high-grade gliomas and correlate with an aggressive tumor subtype, *Neuropathology and Applied Neurobiology*. 44 185–206.2018.
- [66] Q.-Y. Zhong, E.-X. Fan, G.-Y. Feng, Q.-Y. Chen, X.-X. Gou, G.-J. Yue, G. Zhang, A gene expression-based study on immune cell subtypes and glioma prognosis, *BMC Cancer*. 19. 1116.2019.
- [67] J. Lazovic, M.C. Jensen, E. Ferkassian, B. Aguilar, A. Raubitschek, R.E. Jacobs, Imaging immune response in vivo: cytolytic action of genetically altered T cells directed to glioblastoma multiforme, *Clin. Cancer Res*. 14.3832–3839.2008.

- [68] J.G. Smirniotopoulos, F.M. Murphy, E.J. Rushing, J.H. Rees, J.W. Schroeder, Patterns of contrast enhancement in the brain and meninges, *Radiographics*. 27. 525–551. 2007.
- [69] Y. Zhang, J. Wells, R. Buist, J. Peeling, V.W. Yong, J.R. Mitchell, Active inflammation increases the heterogeneity of MRI texture in mice with relapsing experimental allergic encephalomyelitis, *Magn Reson Imaging*. 32.168–174.2014.